

Titanium dioxide doped with transition metals ($M_xTi_{1-x}O_2$, M: Ni, Co): synthesis and characterization for its potential application as photoanode

K. Esquivel · Ma. G. García J. · F. J. Rodríguez ·
M. Vega González · L. Escobar-Alarcón ·
Luis Ortiz-Frade · Luis A. Godínez

Received: 28 July 2010 / Accepted: 18 January 2011 / Published online: 1 February 2011
© Springer Science+Business Media B.V. 2011

Abstract This study presents the synthesis of TiO_2 doped with different amounts of Co and Ni, starting from a simple metallic titanium powder. A successful electrophoretic deposition of these materials on ITO electrodes was achieved for its potential application as photoanodes. EDX, diffuse reflectance UV–Vis spectroscopy, and XRD measurements gave information on the chemical composition of the material and the location of the Ni or Co within the crystal structure of TiO_2 . Raman spectroscopy suggests that for a higher content of doping metal above a defined percentage, the formation of metal oxide is promoted.

A preliminary study of photoelectrocatalytic orange dye degradation shows higher color removal efficiency as compared to the commercial TiO_2 material.

Keywords Ni: TiO_2 · Co: TiO_2 · X-ray diffraction · Rietveld refinement · Raman spectroscopy · Nanocomposites

Introduction

Semiconductor photocatalysis and photoelectrocatalysis have been the subject of many research studies due to the wide range of applications that have been explored for the elimination of hazardous pollutants in air, soil, and water (Han et al. 2009; Zhao et al. 2007; Baea et al. 2008). TiO_2 is particularly popular due to its advantageous characteristics such as high photo activity, thermal and chemical stability, low cost and non-toxicity (Castro et al. 2009). On the other hand, the physical and chemical properties of TiO_2 can be controlled by its particle size, morphology, and crystalline phase (anatase, rutile, and brookite) (Kim et al. 2008).

Nevertheless, the practical applications of TiO_2 are limited by two main issues. While one of them is the low quantum yield that results from the rapid recombination of photo-generated electrons and holes, the other is related to the semiconductor band gap (3.2 eV) that only absorbs effectively 3–4% of the solar energy spectrum (Tian et al. 2009).

K. Esquivel · F. J. Rodríguez · L. Ortiz-Frade ·
L. A. Godínez (✉)
Centro de Investigación y Desarrollo Tecnológico en
Electroquímica, S. C. Parque Tecnológico Querétaro,
Sanfandila, C.P. 76703, Pedro Escobedo, Querétaro,
Mexico
e-mail: lgodinez@cideteq.mx
URL: <http://www.cideteq.mx>

Ma. G. García J.
Universidad de Guanajuato, Calle Lascuráin de Retana,
C.P. 36000, Guanajuato, Guanajuato, Mexico

M. V. González
Centro de Geociencias, Universidad Nacional Autónoma
de México, Campus Juriquilla. Blvd. Juriquilla, 3001,
C.P. 76230, Querétaro, Mexico

L. Escobar-Alarcón
Departamento de Física, Instituto Nacional de
Investigaciones Nucleares, Carr. México-Toluca,
C.P. 52750, Ocoyoacac, Estado de México, Mexico

For these reasons, several studies have been carried out in order to improve the photocatalytic properties of TiO₂. The main approach consists on doping the TiO₂ material with metals such as Fe, Co, Ni, Mn, Au, Ag, and Pt, or with oxides such as WO₃ (Li et al. 2008; Gonçalves et al. 2006; Khaleel and Al-Nayli 2008; Tryba 2008; Glaspell and Manivannan 2005; Sobana et al. 2008; Muruganadham et al. 2006; Tiana et al. 2008). Metals either doped or deposited on TiO₂ are expected to show several effects on the photocatalytic activity due to different mechanisms. For instance, the metal may (i) enhance the electron–hole separation by acting as electron scavenger and (ii) extend the light absorption of the semiconductor material into the visible range. In this way, it has been suggested that a transition metal with a proper oxidation state replaces some of the Ti⁴⁺ centers in the lattice producing an impurity state that reduces the band gap (Kudo et al. 2007; Khan and Kim 2009). In spite of a large quantity of literature dealing with the effect of dopants on the chemical and physical properties of TiO₂, there is very little information available on the location of the dopant within the semiconductor structure and its local environment.

In order to obtain TiO₂ doped with transition metals, several methods have been developed, being the sol–gel method (Garzella et al. 2003; Tian et al. 2009; Piera et al. 2003; Pacheco et al. 2004; Gonçalves et al. 2006; Facchin et al. 2000; Eshaghi et al. 2011; Kisand et al. 2010) the most frequently employed. However, the synthesis of doped TiO₂ starting from metallic titanium mixed with other metals has not been thoroughly explored.

On the other hand, to the best of our knowledge, the preparation of electrophoretically deposited films of TiO₂ modified with cobalt or nickel has not been reported. This approach is advantageous because electrophoretic deposition allows the control of the film thickness, porosity, and roughness factor (Esquivel et al. 2009, Manriquez and Godínez 2007) in a short period of preparation time as compared to spin coating, immersion, or impregnation deposit methods (Kim et al. 2007; Bengtsson et al. 2009; Suriye et al. 2007). Additionally, semiconductor films supported on optically transparent electrodes (OTE) avoid the filtration process that is necessary when photocatalytic degradation tests are carried out in suspension

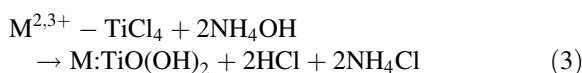
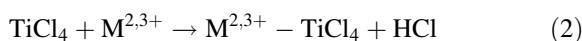
(Barakat et al. 2004; Li et al. 2008; Chu et al. 2008, 2009; Esquivel et al. 2009; Selculi et al. 2004).

In this context, the aim of this study is to prepare and characterize TiO₂ films on OTE doped with Co or Ni using a non-common method that starts from metallic titanium. The obtained deposits were tested for a preliminary photoelectrocatalytic degradation of a model dye (Orange II) in aqueous medium. Additionally, Raman spectroscopy and X-ray diffraction analysis led us to propose the cation location within the TiO₂ lattice.

Materials and methods

M:TiO₂ synthesis

The synthesis method is a modification of those reported previously by Martín et al. (2003). As titanium source, metallic titanium powder (99.7%, Aldrich) was used. A precursor solution was obtained by dissolving the titanium powder in hydrochloric acid (HCl, 36.5–38%, J.T. Baker) under stirring conditions for 3 h at the atmospheric boiling point (1 g Ti/20 mL HCl). Once the titanium tetrachloride was obtained in this reaction mixture, nitric acid (10 vol.%) solution was added drop by drop until a color change was visible (from purple to light yellow). This step indicates the complete oxidation from Ti³⁺ to Ti⁴⁺. Then, the solution was cooled and the dopant salt was added, nickel (as Nickel acetate 99%, Ni(CH₃COO)₂·XH₂O, Alfa Aesar) or cobalt (as Cobalt acetate 98%, Co(CH₃COO)₃·4H₂O, Caledon) at different weight percentages (wt%). For both cations, the wt% used were 5, 20, 40, and 50. Ammonium hydroxide (NH₃ content 28–30%, Sigma-Aldrich) was used as precipitating agent. The powder was filtered and washed several times with deionized water. The TiO₂ modified powder was freeze dried (Free zone 2.5 LABCONCO). The synthetic process with its corresponding chemical equations is presented below (Eqs. 1–3).



Electrophoretic deposition of M:TiO₂ powder on ITO electrodes

M:TiO₂ films were deposited on ITO glass (Indium Tin Oxide, conductive substrate, 1 cm² geometric area) using the electrophoretic method (Manriquez and Godínez 2007). In this way, the glass substrate was immersed for 60 s at room temperature in a previously sonicated colloidal suspension (1 g M:TiO₂ powder in 10 mL Ethyl Alcohol absolute, J.T. Baker), applying a potential difference of 4 V between a stainless steel sheet and the ITO electrode (Esquivel et al. 2009). The modified substrates were then placed in an oven at 550 °C for 3 h in order to obtain the anatase phase of the modified TiO₂ film.

Modified TiO₂ characterization and Rietveld Refinement

Surface morphology analysis of the deposited materials was carried out using scanning electron microscopy (SEM) with a JEOL JSM-5400L microscope. The accelerating voltage employed was 15 kV.

Energy dispersive X-ray spectroscopy (EDX) allowed a rough surface elemental analysis and an approximate atomic relationship between Ti⁴⁺ and the M^{2,3+} species (EDX Oxford Inca X-Sight coupled to a JEOL JSM-6060 LV). Band gap values were determined from UV–Vis diffuse reflectance measurements (Ocean Optics Spectrophotometer) applying the Kubelka–Munk theory (Janczarek et al. 2007). X-ray diffraction analysis (XRD) was performed using a Bruker-AXS D8 advanced diffractometer equipped with a Cu seal tube to generate Cu K_{α1} radiation ($\lambda = 1.5406 \text{ \AA}$) $20 < 2\theta < 60^\circ$ in steps of 0.02° . The collected data were refined by the Rietveld method (Rietveld 1969) using the FULLPROF 05 software, in an attempt to fit the diffraction pattern, in terms of preferred orientation, peak shape, and background. The Thompson–Cox–Hastings pseudo-Voigt function was used to model the peak shape and the preferred orientation. The background was modeled as a polynomial of six refined coefficients. As platform, the Anatase–Rutile template was used. The template was modified by eliminating the rutile phase and varying all the parameters in the next sequence, the scale, background, instrumental, cell and FWHM parameters, preferred orientation, shape, asymmetry,

atomic positions, and the overall B-factor (Torres-Martínez et al. 2008). Raman spectroscopy measurements were acquired with LabRAM HR, Horiba Scientific setup equipped with a Nd:YAG laser ($\lambda = 532 \text{ nm}$ 80 output power 80 mW). The samples were irradiated with a power of 6 mW over a circular area of 1.5 μm diameter of using a microscope set with a 10 \times objective.

Photoelectrocatalysis degradation test

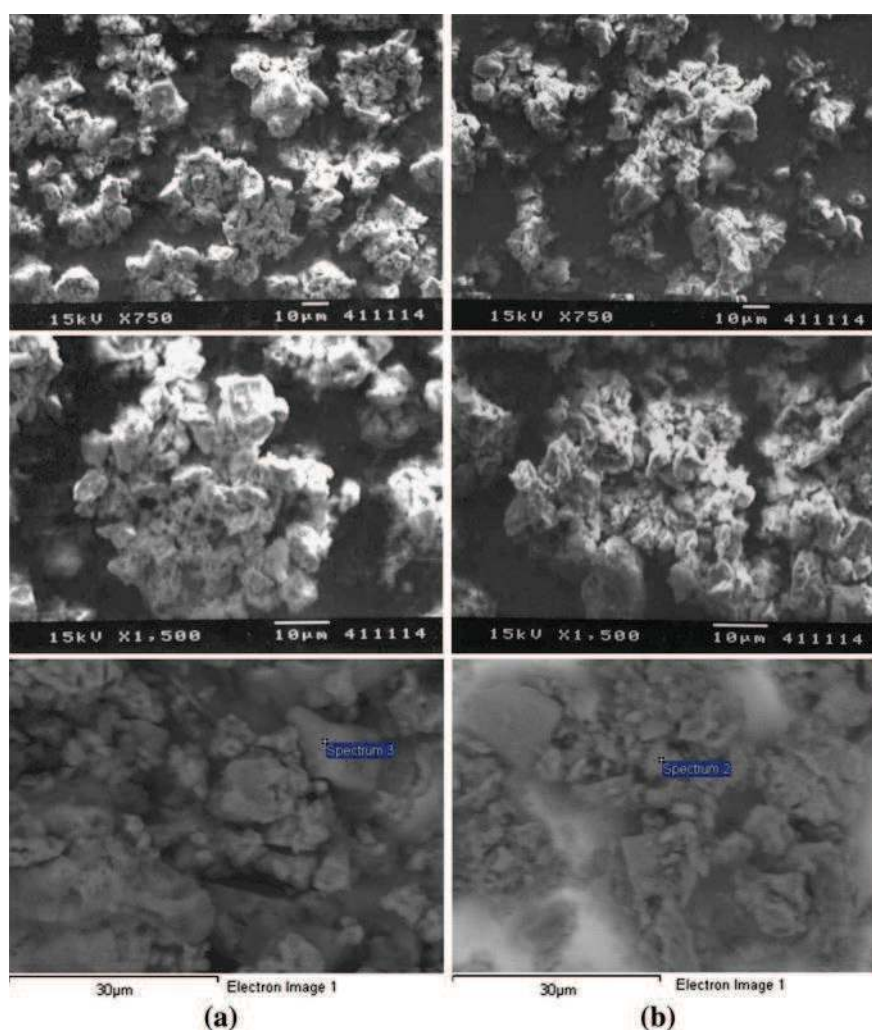
Degradation experiments were carried out using an aqueous solution containing Na₂SO₄ 0.05 M pH 3 as electrolyte and 50 mg L⁻¹ of C₁₆H₁₁N₂NaO₄S (Orange II dye, ALDRICH) as a model dye. In these tests, a vitreous glassy carbon (2 cm² geometric area) was used as working, the M:TiO₂/ITO ($M = 5$ and 20 wt% of Ni and/or Co; 2 cm², geometric area) as counter, and a Hg/Hg₂SO₄ as reference electrode. The experiments were performed under oxygen atmosphere to promote oxygen reduction via two electrons (Esquivel et al. 2009; Peralta-Hernández et al. 2008). The experiments were carried out under potentiostatic conditions applying -0.9 V versus Hg/Hg₂SO₄ (VoltaLab potentiostat/galvanostat, PGZ 301). For the photo-assisted process, the system was illuminated using a low-pressure mercury lamp ($\lambda = 365 \text{ nm}$, $P = 0.75 \mu\text{ cm}^{-2}$). UV–Vis measurements were carried out employing a spectrophotometer (Agilent Technologies) to follow the color disappearing of the model dye species ($\lambda = 487 \text{ nm}$, azo bond).

Results and discussion

Characterization of the Co:TiO₂ and Ni:TiO₂

Scanning electron microscopy images of the modified materials show that the morphology in both semiconductor films (Co, Ni:TiO₂) is characterized by aggregates (clusters) distributed homogeneously over the electrode surface (Fig. 1a, b) (Esquivel et al. 2009; Shieh and Chang 2010). EDX analysis, on the other hand, shows the expected presence of the dopant metal (Co or Ni). An approximation of the mole fraction (X_i) was estimated using the values obtained from EDX analysis, showing that, as expected, an increase in the weight percentage of dopant in the preparation method, results in a larger relationship between the

Fig. 1 SEM images of 20 wt% samples of **a** Co:TiO₂ and **b** Ni:TiO₂ at $\times 750$, $\times 1500$, and $\times 5000$



cation and the titanium species (Table 1). Elemental analysis experiments also showed that in the final material, only a small percentage of the starting quantities of either Ni or Co used is incorporated in the resulting modified substance.

To confirm the presence of the dopant, diffuse reflectance spectroscopy measurements were carried out. The Kubelka–Munk function (Ananpattarachai et al. 2009) shows a decrease in the *band gap* value, an observation that supports the doping of the TiO₂ material. The band gap value obtained for the undoped TiO₂ was 3.1 eV, which is in good agreement with that reported for commercial TiO₂ Degussa P25 (3.2 eV). For the nickel-doped materials, the obtained values show slight changes around 0.1 eV. In this way, the obtained values for the TiO₂-modified materials with

starting Ni amounts of 5, 20, 40, and 50% were 2.5, 2.4, 2.3, and 2.1 eV, respectively. For the cobalt-modified materials, the resulting band gap values were, 2.7, 2.5, 2, and 1.9 eV for 5, 20, 40, and 50 wt% Co, respectively.

A simple inspection of the obtained XRD patterns for all the materials with different weight percentages of Co and Ni did not allow us to establish the presence of these metals. The diffraction angles detected in 2θ (25.3°, 36.96°, 37.82°, 38.6°, 48.04°, 53.92°, and 55.08°) indicates the presence of the crystalline anatase phase (Fig. 2a, b). From the diffraction intensity, a preferential orientation of the plane (101) can be proposed. In the case of samples with a high-amount of dopant (above 40 wt%), new diffraction signals (between 30° and 36° in 2θ) can be

Table 1 Atomic percentage data and mole fraction (X_i), obtained from EDX analysis of the different wt% of Co and Ni doped TiO₂ materials

wt%	X_i (initial weight)	EDS (X_i)	Atomic relationship Co:Ti (final synthesis)
<i>Cobalt</i>			
5	Ti = 0.9613	Ti = 0.3331	1:256
	Co = 0.0390	Co = 0.0013	0.4% Co
	4% Co	O = 0.6663	
20	Ti = 0.8603	Ti = 0.3251	1:26
	Co = 0.1397	Co = 0.0124	3.8% Co
	16.2% Co	O = 0.6625	
40	Ti = 0.7549	Ti = 0.3233	1:23
	Co = 0.2452	Co = 0.0138	4.3% Co
	32.5% Co	O = 0.6627	
50	Ti = 0.7112	Ti = 0.3211	1:17
	Co = 0.2888	Co = 0.0184	5.9% Co
	40.6% Co	O = 0.6605	
wt%	X_i (initial weight)	EDS (X_i)	Atomic relationship Ni:Ti (final synthesis)
<i>Nickel</i>			
5	Ti = 0.9609	Ti = 0.3316	1:122
	Ni = 0.0391	Ni = 0.0027	0.8% Ni
	4% Ni	O = 0.6657	
20	Ti = 0.8600	Ti = 0.3295	1:57
	Ni = 0.1402	Ni = 0.0057	1.8% Ni
	16.3% Ni	O = 0.6645	
40	Ti = 0.7541	Ti = 0.3207	1:16
	Ni = 0.2460	Ni = 0.019	6.3% Ni
	32.6% Ni	O = 0.6603	
50	Ti = 0.7105	Ti = 0.3126	1:10
	Ni = 0.2897	Ni = 0.0311	10% Ni
	40.8% Ni	O = 0.6563	

associated to the rutile phase of TiO₂. This observation is in agreement with previous studies which reported that an increment in the concentration of a doping cation promotes a transformation from the anatase to the rutile phase (Li et al. 2003; Barakat et al. 2005). The fraction of anatase, X_A , in the samples of 40 and 50 wt% was calculated using Eq. 4 (Chen et al. 2008):

$$X_A = \frac{1}{1 + \frac{I_R}{KI_A}}, \tag{4}$$

where K is a constant with a value of 0.79, I_A corresponds to the X-ray intensity at the highest peak

for anatase, and I_R is the intensity at the highest peak for rutile.

The fraction of anatase for samples of 40 wt% of dopant was 0.888 and 0.975 for nickel and cobalt, respectively. For the samples prepared with 50 wt% of dopant, the results were 0.739 and 0.887 for nickel and cobalt, respectively. This information reflects the effect of the increase of the dopant metal amount in the change form anatase to rutile. The XRD measurements were carried out with the material deposited on the ITO glass.

The XRD diffraction pattern of the clean ITO substrate shows signals at 26.48° and 51.56° in 2θ .

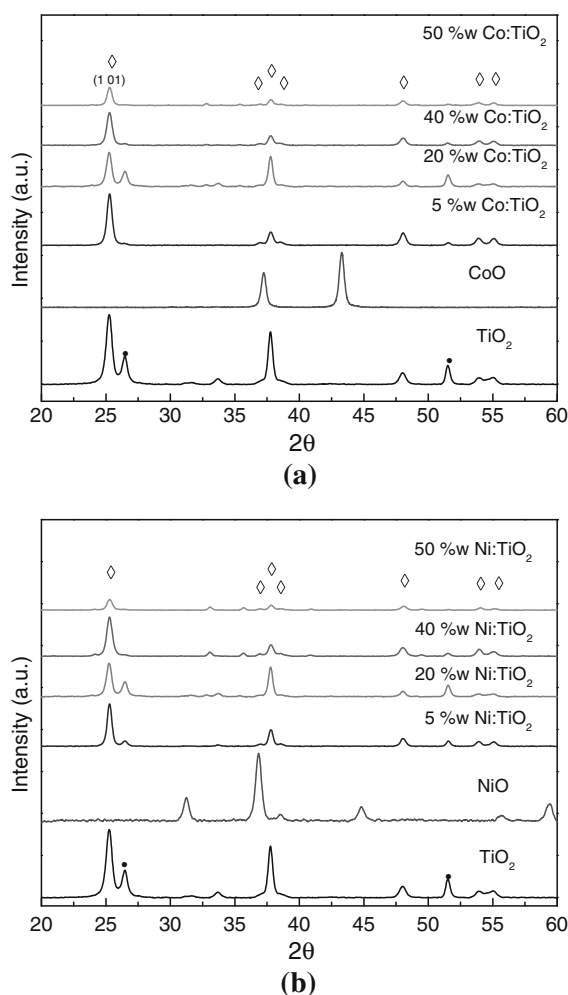


Fig. 2 XRD patterns at different wt% of **a** Co and **b** Ni. *Diamond* is assigned to the anatase phase and *filled circle* to the ITO substrate

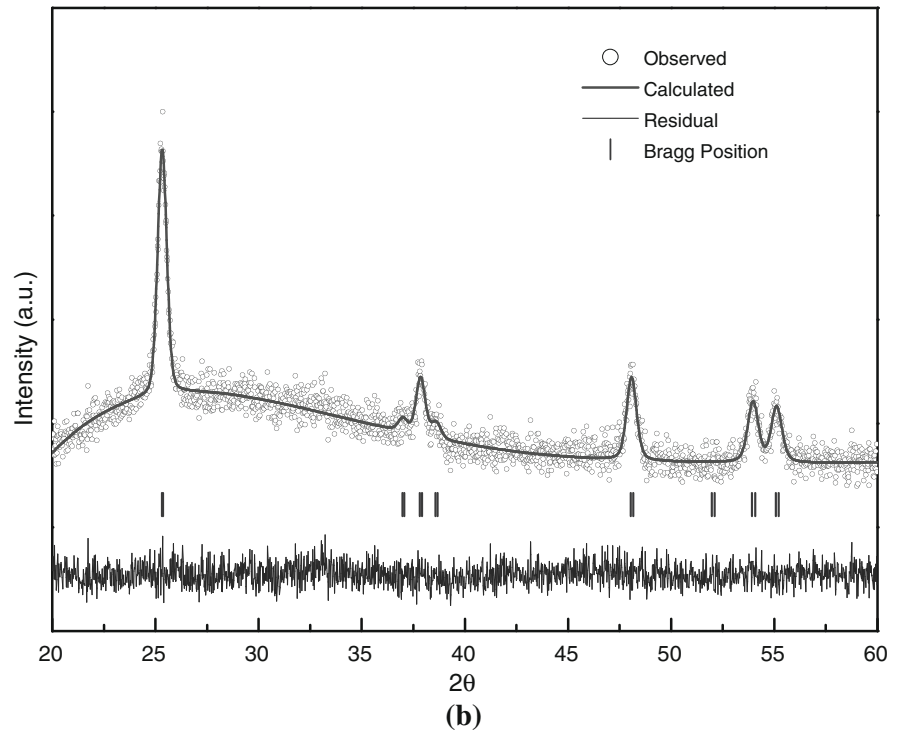
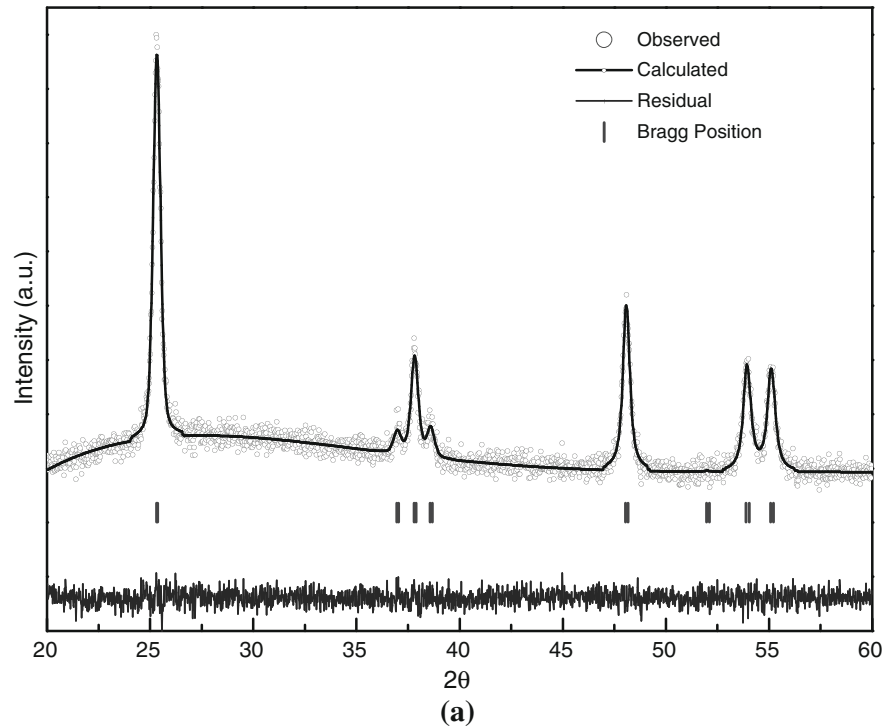
For the modified materials on the other hand, these signals are present in all the diffraction patterns and with larger intensities in the deposits corresponding to 20 wt% of Ni and Co. This is probably related to the higher porosity of these films as compared to the rest of the samples (SEM images not shown). As it was previously mentioned, the surface is formed by clusters (Fig. 1), and as the weight percentage of the dopant increases, the deposit becomes more compact and uniform. The nanometric dimension of these materials was evaluated employing the Debye–Scherrer equation (Chen et al. 2008), and for all the samples under study, an average size value of 18 nm was obtained.

Additionally, XRD patterns corresponding to Ni and Co oxides were obtained in order to check the presence of these species in the modified materials. The results show their absence in the doped semiconductor films. At this point, it can be stated that the cobalt or nickel is present in the deposit but it was not known if it is inside the crystalline structure substituting the titanium(IV) or just present as an interstitial dopant of the anatase structure. Induced-coupled plasma (ICP) measurements ($<0.006 \text{ mg L}^{-1}$), cyclic voltammetry, and polarography showed no presence of nickel or cobalt in solution after electro and photoelectrocatalysis experiments. This fact suggests that the metal is protected inside the TiO_2 structure even in acidic media [the Co and Ni are not stable in acidic mediums (Yang et al. 2009)] or in the presence of H_2O_2 .

Despite that the Rietveld refinement method is mainly used for powder samples, we decided to use it as a first approach for the electrophoretic deposit of $\text{M}:\text{TiO}_2$ in order to propose the possible location of Co^{2+} or Ni^{2+} within the structure of the TiO_2 , (in an interstitial position or as substitution of the Ti^{4+}). In this way, fitting the experimental XRD patterns was carried out assuming that the metal is actually inside the crystalline structure as a substitutional dopant (Li et al. 2005; Djerdj et al. 2006). In Fig. 3a and b, the Rietveld fittings for the samples prepared from 20 wt% of Co and Ni are presented. In these figures, the observed (\circ) and the calculated patterns ($-$) are shown along with the difference between them (residual (Δ)) and the Bragg positions ($|$). The resulting refinement parameters are listed in Table 2a and b. Inspection of this data shows that the Ni or the Co is inserted at the same position of the Ti^{4+} (0, 0.25, and 0.375, x , y , and z) in the anatase structure. It is also interesting to note that the fitting parameter χ^2 is in some cases slightly above 1.3. This difference is probably due to the fact that the collection data were obtained from a diffraction pattern of a deposited film instead of a powder; which can increase the statistical error (Djerdj et al. 2006). When the Ni and/or Co oxide phases were considered on the refinement, no convergence of the method was achieved.

In good agreement with the data reported for the undoped anatase phase (Xu et al. 1999), Raman spectroscopy measurements of the unmodified TiO_2 film showed five typical signals (Figs. 4a, 5a), $146(\text{E}_g)$, $199(\text{E}_g)$, $400(\text{B}_{1g})$, $520(\text{A}_{1g})$, and $643(\text{E}_g) \text{ cm}^{-1}$. When

Fig. 3 Rietveld refinement plot for the 20 wt% samples of **a** Co:TiO₂ and **b** Ni:TiO₂. Observed (○), calculated (—), difference between calculated and observed patterns (Δ) and Bragg positions (|)



the TiO₂ was modified with different amounts of Ni, a slight displacement of the E_g vibration signals (150, 201, and 643 cm⁻¹) was obtained. In the case of Co, a

larger displacement was observed due to the lower crystallinity of the relevant vibrations E_g, B_{1g}, and A_{1g} (157, 206, 402, 519, and 634 cm⁻¹). In addition, it is

Table 2 Rietveld refinement parameters for (a) Co and (b) Ni-doped TiO₂

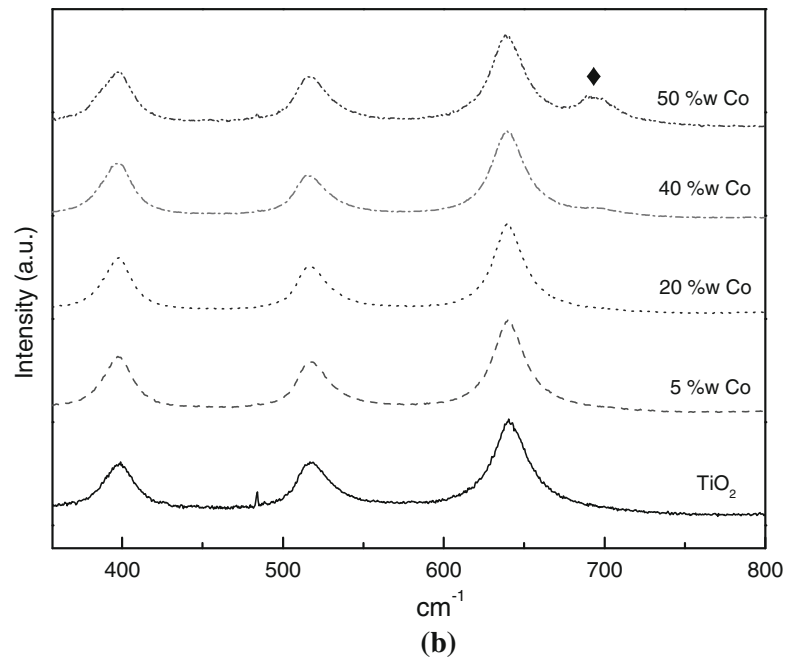
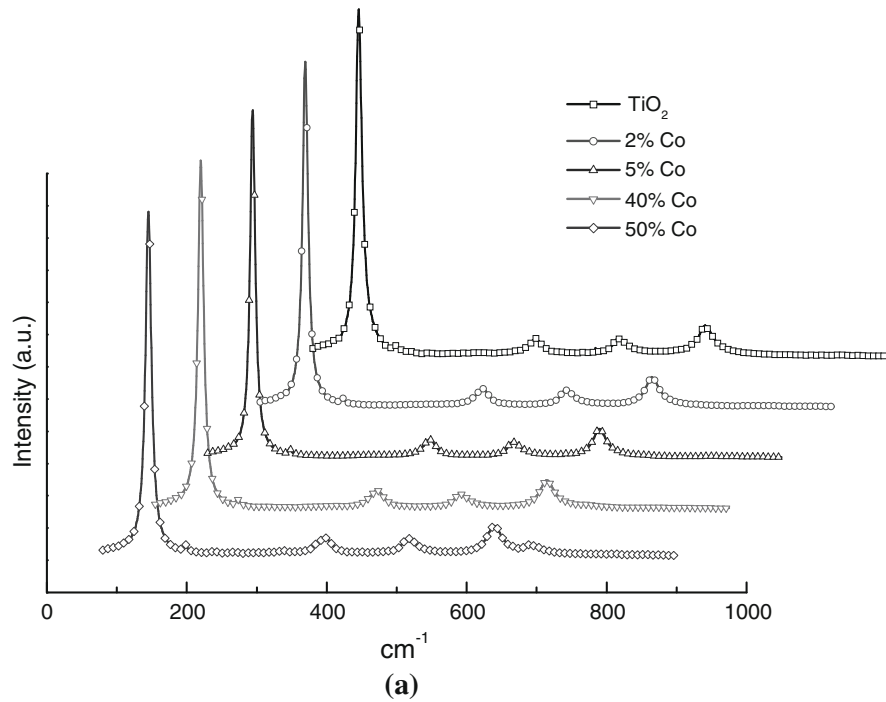
(a) Cobalt				
Sample	5 wt% Co:TiO ₂	20 wt% Co:TiO ₂	40 wt% Co:TiO ₂	50 wt% Co:TiO ₂
Radiation	X-ray (Cu K _α)	X-ray (Cu K _α)	X-ray (Cu K _α)	X-ray (Cu K _α)
Formula	Ti _{0.996} Co _{0.004} O ₂	Ti _{0.961} Co _{0.039} O ₂	Ti _{0.944} Co _{0.056} O ₂	Ti _{0.94} Co _{0.06} O ₂
<i>M</i>	80.08	82.15	83.15	83.38
Temperature/K	298	298	298	298
Crystal system	Tetragonal	Tetragonal	Tetragonal	Tetragonal
Space group	<i>I</i> 41/ <i>amd</i>	<i>I</i> 41/ <i>amd</i>	<i>I</i> 41/ <i>amd</i>	<i>I</i> 41/ <i>amd</i>
<i>a</i> , <i>b</i> /Å	3.7834	3.7844	3.7839	3.7854
<i>c</i> /Å	9.5047	9.5126	9.5043	9.5114
<i>V</i> /Å ³	136.0543	136.2361	136.0831	136.2917
χ ²	2.48	0.771	1.85	1.42
<i>R</i> _{wp}	14.5	26.6	16.8	20.7
<i>R</i> _p	18.8	45.4	24.8	32.5
(b) Nickel				
Sample	5 wt% Ni:TiO ₂	20 wt% Ni:TiO ₂	40 wt% Ni:TiO ₂	50 wt% Ni:TiO ₂
Radiation	X-ray (Cu K _α)	X-ray (Cu K _α)	X-ray (Cu K _α)	X-ray (Cu K _α)
Formula	Ti _{0.992} Ni _{0.008} O ₂	Ti _{0.983} Ni _{0.017} O ₂	Ti _{0.938} Ni _{0.062} O ₂	Ti _{0.989} Ni _{0.11} O ₂
<i>M</i>	80.35	80.84	83.49	86.3
Temperature/K	298	298	298	298
Crystal system	Tetragonal	Tetragonal	Tetragonal	Tetragonal
Space group	<i>I</i> 41/ <i>amd</i>	<i>I</i> 41/ <i>amd</i>	<i>I</i> 41/ <i>amd</i>	<i>I</i> 41/ <i>amd</i>
<i>a</i> , <i>b</i> /Å	3.783	3.7847	3.784	3.7755
<i>c</i> /Å	9.5055	9.5062	9.5016	9.4826
<i>V</i> /Å ³	136.0314	136.1663	136.0489	135.1663
χ ²	3.3	1.07	2.09	1.94
<i>R</i> _{wp}	19.9	44.2	14.5	25.8
<i>R</i> _p	26.5	90.2	19.2	35.8

important to note that for weight percentages larger than 40 wt%, it was possible to observe a new signal located at 694.258 cm⁻¹ for Co: TiO₂ (Fig. 4b) that can be attributed to the A_{1g} mode of Co₃O₄ (Hadjiev et al. 1988). Similarly, for the Ni:TiO₂ materials, this peak appeared at 706.622 cm⁻¹ (Fig. 5b). In this case, the signal could be attributed to NiO according to the Raman Spectra Database of Minerals and Inorganic Materials (RASMIN). These signals are not seen by XRD due to the lack of crystallinity of the relevant oxides and to the detection limit of the equipment. This observation suggests that the TiO₂ structure allows a maximum amount of Ti⁴⁺ substitution by the dopant Ni²⁺ or Co²⁺. The remaining dopant cations are anchored on the TiO₂ surface as another phase, such as Co₃O₄ and/or NiO.

According to all the physico-chemical characterization discussed, the nickel and cobalt species are part of the TiO₂ lattice substituting some of the Ti⁴⁺ centers. In this way, as the dopant material wt% increases, some fraction of this species grows as an oxide outside of the TiO₂ lattice. Additional support comes from the fact that the phase change from anatase to rutile is related to increasing amounts of nickel/or cobalt in the synthetic reaction mixture.

As it has been reported, the highest photocatalytic activity in degradation tests is presented by the anatase phase of the TiO₂ (Yanga et al. 2010; Elsellami et al. 2010; Rauf and Ashraf 2009), and a mixture of phases (anatase-rutile) should then be characterized by a smaller photocatalytic performance. In this context, it was found convenient to

Fig. 4 **a** Raman spectra corresponding to Co:TiO₂ samples with different wt% of the cation and **b** zoom in the 300–800 cm⁻¹ region to show the presence of Co₃O₄ (filled diamond)

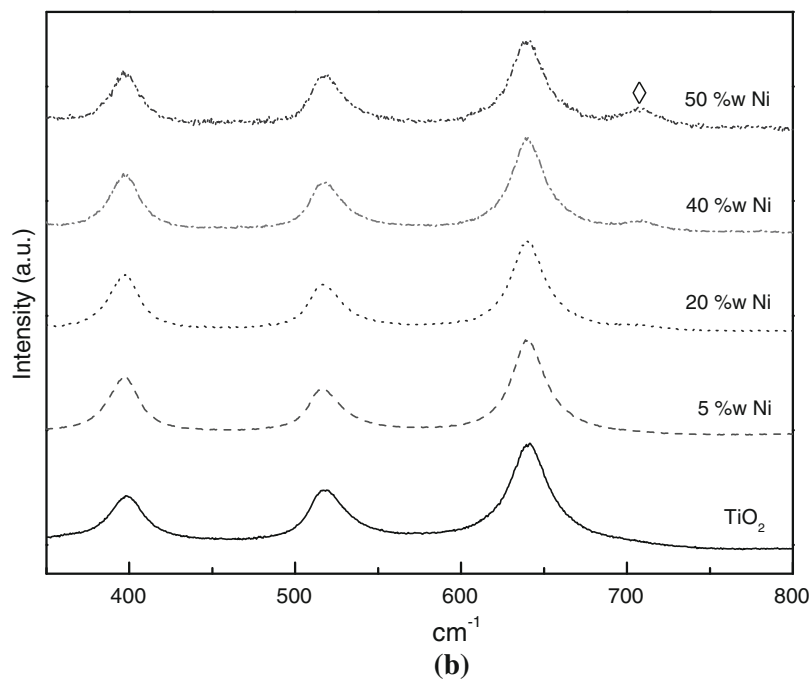
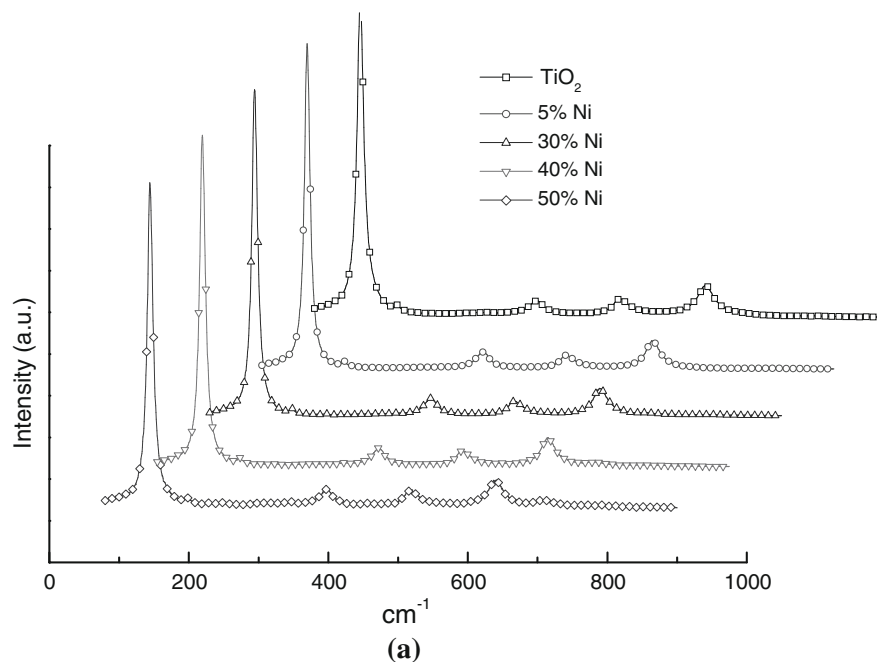


carry out some preliminary experiments on the photoelectrocatalytic degradation of a model dye (azo Orange II) in aqueous solution using the 5 and 20 wt% of the Co and Ni doped materials as photoanodes.

Degradation test using the Co:TiO₂ and Ni:TiO₂ supported on ITO as photoanodes

In the photoelectrochemical experiments for both modified materials (Co and Ni), the color in solution

Fig. 5 **a** Raman spectra corresponding to Ni:TiO₂ samples with different wt% of the cation and **b** zoom in the 300–800 cm⁻¹ region to show the presence of NiO (filled diamond)



was totally removed after 15 min of running the test (Fig. 6). For the non-modified TiO₂, the photoelectrocatalytic activity was substantially lower since the color removal percentage was barely above 50% after 20 min of reaction time. This color removal percentage was achieved with the two modified materials

(20 wt% Co and Ni) after 5 min. For 5 wt% of Co and Ni:TiO₂ on the other hand, the same level of color removal was achieved in 10 and 40 min, respectively. These preliminary experiments suggest that the presence of Ni and Co within the anatase lattice increases the effectiveness of the

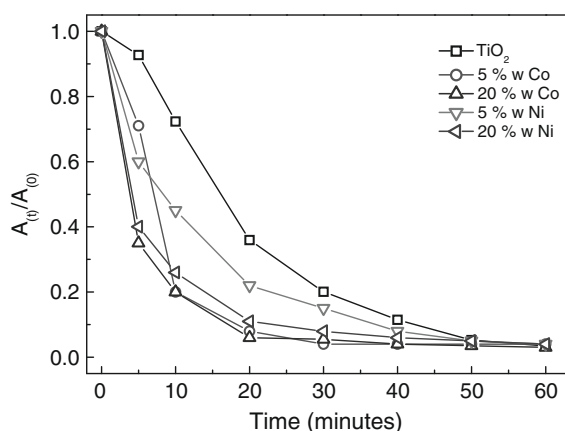


Fig. 6 Absorbance relationships (color removal of orange dye) using TiO₂ and M:TiO₂ materials modified with different wt% of the metallic doping agent (5 and 20 wt% of Co and Ni), [OG II] 50 mg L⁻¹; electrolyte pH 3; 0.05 M Na₂SO₄ solution; degradation time 60 min; UV lamp: $\lambda = 365$ nm, $P = 0.75$ μ W/cm²; $E = -0.9$ V versus Hg/Hg₂SO₄

electrophotocatalytic process as evidenced by a faster color removal rate of the dye Orange II when it is compared to the undoped TiO₂. This observation not only suggests a potential application of these modified semiconductor films as photoanodes in water treatment reactors, but also supports the interpretation of the location of the dopant metals within the semiconductor structure.

Conclusion

It was possible to modify TiO₂, obtained from metallic titanium, with Co and Ni. Also, it was possible to obtain a deposit of the modified materials on a conductive surface by the electrophoretic method. Using the Rietveld refinement, it can be proposed that the Co and Ni are located inside the TiO₂ crystalline anatase structure, substituting some of the titanium (Ti⁴⁺) centers. Raman spectroscopy experiments, on the other hand, showed the presence of the oxides Co₃O₄ and NiO when the starting amount of doping cation was above 40 wt%. In this way, it is possible to suggest that there is some point where Ti⁴⁺ ions cannot be substituted by Ni or Co within the lattice. Since in preliminary photoelectrocatalytic tests, a better performance was observed with these modified materials as compared to the case of undoped TiO₂, this study also suggests that TiO₂

doped with different amounts of Co and Ni can be used in films that constitute a new promising type of photoanodes.

Acknowledgments The authors thank the Mexican Council for Science and Technology (CONACyT, Grant SEP-CONACyT 83894) for financial support of this work. K.E.E. also acknowledges CONACyT for a graduate fellowship and to Eng. Gregorio Solorio^c for his support on the EDX analysis.

References

- Ananpattarachai J, Kajitvichyanukul P, Seraphin S (2009) Visible light absorption ability and photocatalytic oxidation activity of various interstitial N-doped TiO₂ prepared from different nitrogen dopants. *J Hazard Mater* doi: [10.1016/j.jhazmat.2009.02.036](https://doi.org/10.1016/j.jhazmat.2009.02.036)
- Baea S, Shimb E, Yoon J, Joo H (2008) Enzymatic hydrogen production by light-sensitized anodized tubular TiO₂ photoanode. *Solar Energy Mater Solar Cells* 92:402–409
- Barakat MA, Schaeffer H, Hayes G, Ismat SS (2004) Photocatalytic degradation of 2-chlorophenol by Co-doped TiO₂ nanoparticles. *Appl Catal B* 57:23–30
- Barakat MA, Hayes G, Ismat SS (2005) Effect of cobalt doping on the phase transformation of TiO₂ nanoparticles. *J Nanosci Nanotechnol* 10:1–7
- Bengtsson N, Castellote M, Lopez-Muñoz MJ, Cerro L (2009) Preparation of Co-doped TiO₂ for photocatalytic degradation of NO_x in air under visible light. *J Adv Oxid Technol* 12(1):55–64
- Castro AL, Nunes MR, Carvalho MD, Ferreira LP, Jumas JC, Costa FM, Florencio MH (2009) Doped titanium dioxide nanocrystalline powders with high photocatalytic activity. *J Solid State Chem.* doi:[10.1016/j.jssc.2009.04.020](https://doi.org/10.1016/j.jssc.2009.04.020)
- Chen J, Yao M, Wang X (2008) Investigation of transition metal ion doping behaviours on TiO₂ nanoparticles. *J Nanopart Res* 10:163–171
- Chen L-C, Ho Y-C, Guo W-S, Huang C-M, Pan T-C (2009) Enhanced visible light-induced photoelectrocatalytic degradation of phenol by carbon nanotube-doped TiO₂ electrodes. *Electrochim Acta* 54:3884–3891
- Chu D, Yuan X, Qin G, Xu M, Zheng P, Lu J, Zha L (2008) Efficient carbon-doped nanostructured TiO₂ (anatase) film for photoelectrochemical solar cells. *J Nanopart Res* 10:357–363
- Djerdj I, Tonejc AM, Tonejc A (2006) Structural refinement of nanocrystalline TiO₂ samples. *Electron Crystallogr* 497–501
- Elsellami L, Vocanson F, Dappozze F, Puzenat E, Paisse O, Houas A, Guillard C (2010) Kinetic of adsorption and of photocatalytic degradation of phenylalanine effect of pH and light intensity. *Appl Catal A* 380:142–148
- Eshaghi A, Mozaffarinia R, Pakshir M, Eshaghi A (2011) Photocatalytic properties of TiO₂ sol-gel modified nanocomposite films. *Ceram Int* 37:327–331
- Esquivel K, Arriaga LG, Rodríguez FJ, Martínez L, Godínez LA (2009) Development of a TiO₂ modified optical fiber electrode and its incorporation into a photoelectrochemical reactor for wastewater treatment. *Water Res* 43:3593–3603

- Facchin G, Carturan G, Campostrini R, Gialanella S, Lutterotti L, Armelao L, Marci G, Palmisano L, Sclafani A (2000) Sol-gel synthesis and characterisation of TiO₂-anatase powders containing nanometric platinum particles employed as catalysts for 4-nitrophenol photodegradation. *J Sol-Gel Sci Technol* 18:29–59
- Garzella C, Bontempi E, Depero LE, Vomiero A, Della Mea G, Sberveglieri G (2003) Novel selective ethanol sensors: W/TiO₂ thin films by sol-gel spin-coating. *Sens Actuators B* 93:495–502
- Glaspell G, Manivannan A (2005) Sol-gel synthesis and magnetic studies of titanium dioxide doped with 10% M (M = Fe, Mn and Ni). *J Clust Sci* 16(4):501–513
- Gonçalves G, Lenzi MK, Santos OAA, Jorge LMM (2006) Preparation and characterization of nickel based catalysts on silica, alumina and titania obtained by sol-gel method. *J Non-Cryst Solids* 352:3697–3704
- Hadjiev VG, Iliev MN, Vergilov IV (1988) The Raman spectra of Co₃O₄. *J Phys C* 21:L199–L201
- Han F, Subba Rao KV, Srinivasan M, Dharmarajan R, Naidu R (2009) Tailored titanium dioxide photocatalysts for the degradation of organic dyes in wastewater treatment: a review. *Appl Catal A* 359:25–40
- Janczarek M, Kisch H, Hupka J (2007) Photoelectrochemical characterization of nitrogen-modified TiO₂. *Physicochem Probl Miner Process* 41:159–166
- Khaleel A, Al-Nayli A (2008) Supported and mixed oxide catalysts based on iron and titanium for the oxidative decomposition of chlorobenzene. *Appl Catal B* 80:176–184
- Khan R, Kim T-J (2009) Preparation and application of visible-light-responsive Ni-doped and SnO₂-coupled TiO₂ nanocomposite photocatalysts. *J Hazard Mater* 163:1179–1184
- Kim HR, Choi KY, Shul Y-G (2007) Preparation of TiO₂/SiO₂ hollow spheres and their activity in methylene blue photodecomposition. *Korean J Chem Eng* 24(4):596–599
- Kim DH, Choi D-K, Kim S-J, Lee KS (2008) The effect of phase type on photocatalytic activity in transition metal doped TiO₂ nanoparticles. *Catal Commun* 9:654–657
- Kisand V, Joost U, Reedo V, Pärna R, Tätte T, Shulga J, Saar A, Matisen L, Kikas A, Kink I (2010) Influence of the heating temperature on the properties of nickel doped TiO₂ films prepared by sol-gel method. *Appl Surf Sci* 256:4538–4542
- Kudo A, Niishiro R, Iwase A, Kato H (2007) Effects of doping of metal cations on morphology, activity, and visible light response of photocatalysts. *Chem Phys* 339:104–110
- Li X, Yue P-L, Kutal C (2003) Synthesis and photocatalytic oxidation properties of iron doped titanium dioxide nanosemiconductor particles. *New J Chem* 27:1264–1269
- Li W, Frenkel AI, Woicik JC, Ni C, Ismat SS (2005) Dopant location identification in Nd³⁺-doped TiO₂ nanoparticles. *Phys Rev B* 72:155315-1–155315-6
- Li J, Liu S, He Y, Wang J (2008) Adsorption and degradation of the cationic dyes over Co doped amorphous mesoporous titania-silica catalyst under UV and visible light irradiation. *Microporous Mesoporous Mater* 115:416–425
- Manriquez J, Godínez LA (2007) Tuning the structural, electrical and optical properties of Ti(III)-doped nanocrystalline TiO₂ films by electrophoretic deposition time. *Thin Solid Films* 515:3402–3413
- Martín C, Solana G, Malet P, Rives V (2003) Nb₂O₅-supported WO₃: a comparative study with WO₃/Al₂O₃. *Catal Today* 78:365–376
- Muruganadham M, Swaminathan M (2006) Nano-Ag particles doped TiO₂ for efficient photodegradation of direct azo dyes. *J Mol Catal A* 258:124–132
- Pacheco F, González M, Medina A, Velumani S, Ascencio JA (2004) Structural analysis of cobalt titanate nanoparticles obtained by sol-gel process. *Appl Phys A* 78:531–536
- Peralta-Hernández JM, Meas-Vong Y, Rodríguez FJ, Chapman TW, Maldonado MI, Godínez LA (2008) Comparison of hydrogen peroxide-based processes for treating dye-containing wastewater: decolorization and destruction of Orange II azo dye in dilute water. *Dyes Pigments* 76:656–662
- Piera E, Tejedor-Tejedor MI, Zorn ME, Anderson MA (2003) Relationship concerning the nature and concentration of Fe(III) species on the surface of TiO₂ particles and photocatalytic activity of the catalyst. *Appl Catal B* 46:671–685
- Raman Spectra Database of Minerals and Inorganic Materials (RASMIN) at RIO-DB of AIST (http://www.aist.go.jp/RIODB/rasmin/E_index.htm)
- Rauf MA, Ashraf SS (2009) Review: fundamental principles and application of heterogeneous photocatalytic degradation of dyes in solution. *Chem Eng J* 151:10–18
- Rietveld HM (1969) A profile refinement method for nuclear and magnetic structures. *J Appl Crystallogr* 2:65–71
- Selculi H, Zaltner W, Sene JJ, Bekbolet M, Anderson MA (2004) Photocatalytic and photoelectrocatalytic performance of 1% Pt doped TiO₂ for the detoxification of water. *J Appl Electrochem* 34:653–658
- Shieh Y-N, Chang Y-Y (2010) Influence of cobalt ion implantation on optical properties of titanium dioxide thin films. *Thin Solid Films* 518:7464–7467
- Sobana SJ, Qiao L, Sun S, Wang G (2008) Photocatalytic degradation of Orange G on nitrogen-doped TiO₂ catalysts under visible light and sunlight irradiation. *J Hazard Mater* 155:312–319
- Suriye K, Praserthdam P, Jongsomjit B (2007) Effect of surface sites of TiO₂ support on the formation of cobalt-support compound in Co/TiO₂ catalysts. *Catal Commun* 8:1772–1780
- Tian B, Li C, Gu F, Jiang H (2009) Synergetic effects of nitrogen doping and Au loading on enhancing the visible-light photocatalytic activity of nano-TiO₂. *Catal Commun* 10:925–929
- Tiana H, Maa J, Li K, Li J (2008) Photocatalytic degradation of methyl orange with W-doped TiO₂ synthesized by a hydrothermal method. *Mater Chem Phys* 112:47–51
- Torres-Martínez LM, Juárez-Ramírez I, Del Ángel-Sánchez K, Garza-Tovar L, Cruz-López A, Del Ángel G (2008) Rietveld refinement of sol-gel Na₂Ti₆O₁₃ and its photocatalytic performance on the degradation of methylene blue. *J Sol-Gel Sci Technol* 47:158–164
- Tryba B (2008) Immobilization of TiO₂ and Fe–C–TiO₂ photocatalysts on the cotton material for application in a flow photocatalytic reactor for decomposition of phenol in water. *J Hazard Mater* 151:623–627
- Xu W-X, Zhu S, Fu X-C, Chen Q (1999) The structure of TiO_x thin film studied by Raman spectroscopy and XRD. *Appl Surf Sci* 148:253–262

- Yang Q, Choi H, Al-Abed SR, Dionysiou DD (2009) Iron–cobalt mixed oxide nanocatalysts: heterogeneous peroxymonosulfate activation, cobalt leaching, and ferromagnetic properties for environmental applications. *Appl Catal B* 88:462–469
- Yanga H, Ana T, Li G, Song W, Cooper WJ, Luo H, Guo X (2010) Photocatalytic degradation kinetics and mechanism of environmental pharmaceuticals in aqueous suspension of TiO₂: a case of β blockers. *J Hazard Mater* 179:834–839
- Zhao H, Jiang D, Zhang S, Wen W (2007) Photoelectrocatalytic oxidation of organic compounds at nanoporous TiO₂ electrodes in a thin-layer photoelectrochemical cell. *J Catal* 250:102–109